



ORIGINAL ARTICLE

Investigation of anti-human ovarian cancer effects of decorated Au nanoparticles on *Thymbra spicata* extract modified Fe₃O₄ nanoparticles



Wenqing Ding^a, Zhengqiao Liang^b, Attalla F. El-Kott^{c,d,*}, Ayman E. El-Kenawy^e

^a Department of Gynecology, Longgang District Maternity&Child Healthcare Hospital of Shenzhen City, Shen zhen 518172, China

^b Department of Ultrasound Medicine, Longgang District Maternity&Child Healthcare Hospital of Shenzhen City, Shen zhen 518172, China

^c Biology Department, College of Science, King Khalid University, Abha 61413, Saudi Arabia

^d Zoology Department, College of Science, Damanhour University, Damanhour 22511, Egypt

^e Pathology Department, College of Medicine, Taif University, Taif 11099, Saudi Arabia

Received 8 January 2021; accepted 2 May 2021

Available online 8 May 2021

KEYWORDS

Ultrasound;
Magnetic;
Gold;
Human ovarian cancer

Abstract This work describes an eco-friendly approach for *in situ* immobilization of Au nanoparticles on the surface of Fe₃O₄ nanoparticles, with the help of *Thymbra spicata* extract and ultrasound irradiations, without using any toxic reducing and capping agents. The combination of Fe₃O₄ NPs and Au NPs in one hybrid nanostructure (Fe₃O₄@*Thymbra spicata*/Au NPs) represents a promising strategy for targeted biomedical applications. The structure, morphology, and physicochemical properties were characterized by various analytical techniques such as fourier transformed infrared spectroscopy (FT-IR), field emission scanning electron microscopy (FESEM), transmission electron microscopy (TEM), energy dispersive X-ray spectroscopy (EDS), X-ray diffraction (XRD), inductively coupled plasma (ICP) and vibrating sample magnetometer (VSM). MTT assay was used on common ovarian cancer cell lines i.e., SW-626, PA-1, and SK-OV-3 to survey the cytotoxicity and anti-ovarian cancer effects of Fe₃O₄@*Thymbra spicata*/Au NPs. The best results of cytotoxicity and anti-ovarian cancer properties were seen in the concentration of 1000 µg/mL. Fe₃O₄@*Thymbra spicata*/Au NPs had very low cell viability and high anti-ovarian cancer activities dose-dependently against PA-1, SW-626, and SK-OV-3 cell lines without any cytotoxicity on the normal cell line (HUVEC). For investigating the antioxidant properties of Fe₃O₄@*Thymbra spicata*/Au NPs, the DPPH test was used in the presence of butylated hydroxy-

* Corresponding author at: Biology Department, College of Science, King Khalid University, Abha 61413, Saudi Arabia.

E-mail address: elkottaf@yahoo.com (A.F. El-Kott).

Peer review under responsibility of King Saud University.



Production and hosting by Elsevier

toluene as the positive control. $\text{Fe}_3\text{O}_4@Thymbra\ spicata/\text{Au}$ NPs inhibited half of the DPPH molecules in the concentration of 107 $\mu\text{g}/\text{mL}$. Maybe significant anti-human ovarian cancer potentials of $\text{Fe}_3\text{O}_4@Thymbra\ spicata/\text{Au}$ NPs against common human ovarian cancer cell lines are linked to their antioxidant activities. After confirming the above results in the clinical trial researches, this formulation can be administrated for the treatment of several types of human ovarian cancers in humans.

© 2021 Published by Elsevier B.V. on behalf of King Saud University. This is an open access article under the CC BY-NC-ND license (<http://creativecommons.org/licenses/by-nc-nd/4.0/>).

1. Introduction

Ovarian cancer, as one of the common cancers in women, has been distributed in both developing and developed countries. The main risk factors of ovarian cancer are family history, age, reproductive history, breast cancer, hormone therapy, obesity and overweight, gynecologic surgery, human papillomavirus, and talcum powder (GBD, 2015; Mortality, 2015). At first, ovarian cancer arises with growing an abnormal cell and after a while it spread in all parts of the uterine and all parts of the body (Mortality, 2015). The symptoms of ovarian cancer are pain or pressure in the pelvis, pain in the back or abdomen, feeling full rapidly when eating, changes in bowel habits such as constipation, unexpected vaginal bleeding, bloating, changes in urination patterns such as more frequent urination, and maybe nausea and indigestion, appetite loss, weight loss, breathlessness, and fatigue (Ebell et al., 2016). Blood tests, imaging examination, laparoscopy, and biopsy are used to diagnose ovarian cancers in several stages of cancer including localized, regional, and distant (Grossman, 2018). For the treatment of ovarian cancer, chemotherapy, radiation therapy, and immunotherapy are used (Gibson et al., 2016). Due to severe side effects of the chemotherapeutic drugs and supplements, the formulation of the chemotherapeutic medications from metallic nanomaterial's especially Au nanoparticles and hybrid biomolecular functionalized magnetic nanomaterials are the research priority of pharmacology, oncology, and organic chemistry researchers (Ghashghaii et al., 2017; Abdoli et al., 2020; Mahdavi et al., 2020).

Nanomaterials, which are the subject of our study, have unique competencies different from their macro-scale counterparts due to their low volume/surface ratio and many advanced as well as some physiochemical criteria such as color, solubility, strength, prevalence, toxicity, magnetic, optical, thermodynamics (Gawande et al., 2013; Lotfi and Veisi, 2019; Sanli et al., 2020). In recent years, biological methods which are basically non-toxic, cost-effective, and environmentally friendly have gained much interest compared to physicochemical nanoparticle synthesis methods (Rossi et al., 2014; Veisi et al., 2019; Hemmati et al., 2020; 2011). Various pathways have been developed for the biogenic or biological formulation of nanomaterials from the salts of different metal ions. The synthesis of nanoparticles under purely 'green' principles can be achieved using an environmentally compatible solvent system with environmentally-friendly stabilizing and reducing factors (Baghayeri et al., 2018; Veisi et al., 2015; Katifelis et al., 2020; Katifelis et al., 2018; Cheng et al., 2019). The basic principle in the biogenesis of nanoparticles is reducing metal ions of several biomolecules found in vital organisms. In addition to reducing the environmental impact of biological

synthesis, this critical step enables the production of large quantities of nanoparticles, which are well-defined in size and morphology, and independent of contamination, as well. Microorganisms, marine algae, plant extracts, plant tissue, fruits, and all plants are administrated to formulate nanomaterials (Lotfi and Veisi, 2019; Sanli et al., 2020; Rossi et al., 2014; Veisi et al., 2019). The green synthesized metallic nanoparticles have achieved notable consideration in various medicinal disciplines (Gawande et al., 2013; Lotfi and Veisi, 2019; Sanli et al., 2020; Rossi et al., 2014). Some relevant conducted studies have shown that some nanoparticles (Especially platinum, gold, and silver nanoparticles) have promising therapeutic properties accounting for their potential use as excellent alternatives to physicochemically different metal-supported nanoparticles, antibacterial, and particularly anticancer drugs (Such as Cisplatin and Azathioprine) (Katifelis et al., 2020; Katifelis et al., 2018; Cheng et al., 2019; Mirfakhraei et al., 2018). The previous studies have indicated the anticancer effects of metallic nanoparticles against various cell lines such as Lewis lung carcinoma (LL2) cells, ADR/MCF-7 cancer cells, A549 lung epithelial cancer cell line, HT29, HCT15, HCT116, and RKO colon cancer cell lines, U87 and LN229 human glioma cancer lines, A549 cells and HeLa cells, HepG2-R, HDF together with C0045C, 4 T1 mouse mammary carcinoma and A549, H460, and H520 human lung cancer cells (Abdoli et al., 2020; Mahdavi et al., 2020).

Recently, nanostructures with combined diagnostic and therapeutic functions represent a potential application for tumor therapy (Li et al., 2014; Mu et al., 2017). Many inorganic nanoparticles with various compositions, physical features, and functionalities have been widely synthesized and used as drug vehicles (Lian et al., 2012). Likewise, metal nanoparticles and their oxides with special shapes (sphere, tadpole, and pearl chain) have been successfully generated. Magnetic nanoparticles (MNPs), such as iron oxide, have been widely studied because of their combination of properties such as superparamagnetism, biocompatibility, and ease of synthesis. The most common form of iron oxide used is magnetite (Fe_3O_4) with a tendency to oxidize, which alters its magnetic properties (Mcnamara and Tofail, 2015). That is why iron oxide nanoparticles are generally coated with a biocompatible layer such as polymers, silica, or gold (Au) (Tassa et al., 2011; Lutz et al., 2006; Kohler et al., 2004; Masoudi et al., 2012; Ban et al., 2005; Chen et al., 2003; Zhou et al., 2011). Moreover, impregnation of noble metals over Fe_3O_4 biocomposites introduces some synergistic properties that augment their potential applications. They have been wonderfully implemented in diverse fields such as sensing, adsorption, degradation of dyes and contaminants, disposal of heavy and toxic metals, drug delivery, biomedical applications and cancer therapy (Awual

et al., 2018; Veisi, 2019; Hamelian et al., 2018; Katata-Seru et al., 2018; Sangami and Manu, 2017; Beheshtkhoo et al., 2018; Radini et al., 2018; Ángeles-Pascual et al., 2018). Among the different noble metal nanoparticles, Au NPs are relatively cheaper as compared to Pt. Based on their distinct characteristics the Au NPs individually find multilayered applications in the different arena like health, medicine, animal husbandry, agriculture, household, packaging, optics, electronics and catalysis (Lotfi and Veisi, 2019; Veisi, 2019).

The unique coalescence of Au NPs and Fe₃O₄ has found a broad range of utility in biological targeting, biological separation and high-density magnetic recording (Baghayeri et al., 2018; Veisi et al., 2015; Katifelis et al., 2020; Katifelis et al., 2018; Cheng et al., 2019; Mirfakhraei et al., 2018). We wish to report the synthesis, characterizations and applications of novel Au NPs decorated *Thymbra spicata* extract modified-magnetite nanocomposite (Fe₃O₄@*Thymbra spicata*/Au) with the help of ultrasonic irradiation for the first time. The biomolecules of extract afford additional stability to the MNPs from unwanted oxidation and corrosion (Awual et al., 2018; Veisi, 2019; Hamelian et al., 2018; Katata-Seru et al., 2018; Sangami and Manu, 2017; Beheshtkhoo et al., 2018; Radini et al., 2018). The modified surface can easily have capped the gold ions and *in situ* reduced and stabilized them without aggregations (Scheme 1). It demonstrated excellent potential in biological applications. So, we extended our material in the bio-assay against common human ovarian cancer cell lines i.e., PA-1, SW-626, and SK-OV-3 for the first time.

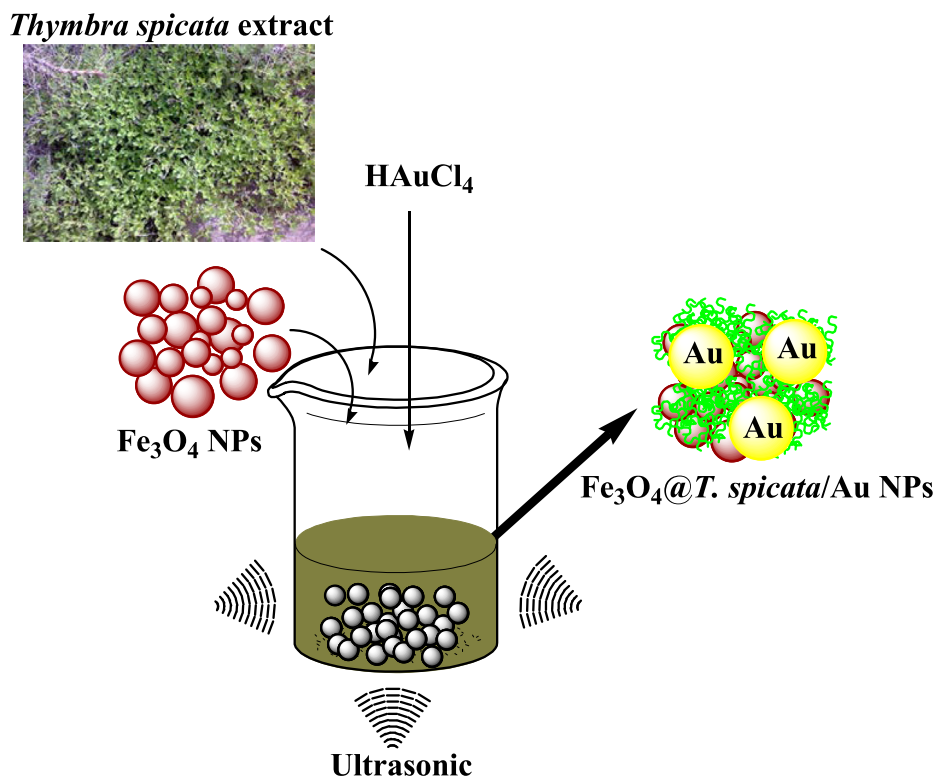
2. Experimental

2.1. Materials and apparatus

All the reagents were purchased from Aldrich and Merck and were used without any purification. In instrumental section, the particle size, morphology and atomic mapping analysis of the nanomaterial was investigated using a FESEM-TESCAN MIRA3 microscope equipped with EDX. The crystalline structures of the samples were evaluated by X-ray diffraction (XRD) analysis on a Bruker D8 Advance diffractometer with CuK α radiation at 40 kV and 20 mA. Fourier transform infrared (FT-IR) spectra were recorded with a Perkin Elmer 65 spectrometer in the range of 400–4000 cm⁻¹. Transmission electron microscopy (TEM) analysis was performed on a Phillips CM10 microscope at an accelerating voltage of 200 kV. Magnetization measurements were carried out on a BHV-55 vibrating sample magnetometer (VSM).

2.2. Preparation of *Thymbra spicata* leaf extract

One hundred grams of *Thymbra spicata* dried leaves were ground and heated at 70 °C with 500 mL of sterile distilled water for 2 h. Afterward, the mixture was cooled down to room temperature. The aqueous extract of *Thymbra spicata* leaves was centrifuged at 6500 rpm. Moreover, the supernatant was separated by filtration and was kept in a refrigerator at 4°C for later investigations.



Scheme 1 Schematic fabrication of Fe₃O₄@*Thymbra spicata*/Au NPs mediated by *Thymbra spicata* extract under ultrasonic irradiations.

2.3. Preparation of the biologically active magnetic $Fe_3O_4@Thymbra\ spicata/Au$ nanocomposite

The magnetic Fe_3O_4 nanoparticles were prepared by the chemical co-precipitation method according to the literature [18b]. In the first step, magnetite nanoparticle (0.5 g) was dispersed in 100 mL water and sonicated for 20 min at 60 °C. Next, the *Thymbra spicata* extract was added to the mixture. Afterward, the solution was sonicated again at this temperature for 60 min, and subsequently, a solution of $H AuCl_4$ in water was added dropwise using a dropping funnel in the reaction media (0.02 g, 10 mL, the drip rate was 1 mL/min) under sonication. After complete addition, the reaction continued for another 60 min under ultrasonic conditions. Then, the mixture was cooled to room temperature and the magnetic nanoparticles $Fe_3O_4@Thymbra\ spicata/Au$ as a black reddish solid were isolated from the solution by magnetic separation and washed several times by DI water and ethanol. The final nanocomposite was dried in a vacuum at 40 °C. The concentration of gold was 0.12 mmol/g, which was determined by ICP-OES.

2.4. Determination of anti-human ovarian cancer properties of $Fe_3O_4@Thymbra\ spicata/Au$ NPs nanocomposite

In this assay, following human ovarian cell lines and the normal cell line (HUV EC) were used to study the cytotoxicity and anticancer potential of human ovarian over the $Fe_3O_4@Thymbra\ spicata/Au$ NPs nanocomposite using the common cytotoxicity test i.e., MTT assay *in vitro* condition:

- a) Normal cell line: HUV EC.
- b) Human ovarian cancer cell lines: PA-1, SW-626, SK-OV-3.

The cells were cultured as a monolayer culture in 90% RPMI-1640 medium and 10% fetal serum and were immediately after supplemented with 200 mg/mL streptomycin, 125 mg/mL penicillin, and 8 mg/mL amphotericin B. The culture was then exposed to 0.5 atmospheric carbon dioxide at 37 °C, on which the tests were performed after at least ten successful passages. MTT was an assay used to investigate the toxic effects of various materials on various cell lines, including non-cancer and cancer cells. To evaluate the cell toxicity effects of the compounds used in this research, the cells were transferred from the T25 flask to the 96-well flasks. In each cell of the 96-cell flasks, 7000 cells of cancer and fibroblast cell lines were cultured, and the volume of each cell was eventually increased to 100 μ L. Before treating the cells in the 96-well flask, the density of cells was increased to 70%, so the 96-well flasks were incubated for 24 h to obtain the cell density of 7×10^3 . Thereafter, the initial culture medium was discarded, and variable concentrations (0–1000 μ g/mL) of $Fe_3O_4@Thymbra\ spicata/Au$ NPs nanocomposite were incubated at 37 °C and 5% CO_2 for 24, 48, and 72 h. Then, 20 μ L MTT was added to each well. This step was followed by the addition of 100 μ L of DMSO solvent to each well. The treated wells were then kept at room temperature for 25 min and read at 490 and 630 nm by a microtitre plate reader. The cell lines were also treated with the hydroalcoholic extract (1.25 mg/mL), which inhibited about 20% of the cell growth. Annexin/PI method was used to determine the apoptosis level in the treated and control cell lines using a flow cytometry

machine. Under the optimized experimental conditions, the cell lines were treated with variable concentrations (0–1000 μ g/mL) of $Fe_3O_4@Thymbra\ spicata/Au$ NPs nanocomposite for 24 h. Cells were irrigated with phosphate-buffered saline (PBS). After centrifugation, buffer binding was added to the obtained precipitate. Then, 5 μ L Annexin V dye was added and incubated for 15 min at 25 °C. Cells were washed with the binding solution, following by the addition of 10 μ L of PI dye. Finally, cell analysis was conducted by a flow cytometry machine according to the below formula (Abdoli et al., 2020; Mahdavi et al., 2020):

$$\text{Cell viability (\%)} = \frac{\text{Sample A}}{\text{Control A}} \times 100$$

2.5. Determination of the antioxidant activities of $Fe_3O_4@Thymbra\ spicata/Au$ NPs nanocomposite

To study the radical scavenging antioxidant property of our $Fe_3O_4@Thymbra\ spicata/Au$ NPs, DPPH (2,2-diphenyl-1-picrylhydrazyl) is being used (Ghashghaii et al., 2017; Abdoli et al., 2020; Mahdavi et al., 2020).

A 39.4% DPPH solution (w/v) was prepared in 1:1 aqueous MeOH. Simultaneously, different samples of $Fe_3O_4@Thymbra\ spicata/Au$ NPs nanocomposite of variable concentrations (0–1000 μ g/mL) were prepared. The DPPH solution was then added to $Fe_3O_4@Thymbra\ spicata/Au$ NPs nanocomposite samples and incubated at 37 °C. After 30 min of incubation, the absorbances of the mixtures were measured at 570 nm. MeOH (50%) and butylated hydroxytoluene (BHT) were considered as negative and positive controls respectively in the study. The antioxidant properties of $Fe_3O_4@Thymbra\ spicata/Au$ NPs nanocomposite were determined in terms of % inhibition and expressed as

$$\text{Inhibition (\%)} = \frac{\text{Sample A}}{\text{Control A}} \times 100$$

Calculation of half-maximal inhibitory concentration (IC_{50}) is a suitable method for comprising the activity of pharmaceutical-based materials. In this method, the measurement and comparison criterion is the concentration in which 50% of the final activity of the drug occurs. In this experiment, the IC_{50} of various repeats is estimated and compared with the IC_{50} of BHT, which is introduced as the antioxidant activity index. The closer is the obtained value to the IC_{50} of BHT, the stronger is the antioxidant activity of the material. The graph of the IC_{50} of the extract was produced by drawing the percent inhibition curve versus the extract concentration. First, three stock samples with variable concentrations (0–1000 μ g/mL) of $Fe_3O_4@Thymbra\ spicata/Au$ NPs nanocomposite were prepared. Then, a serial dilution was prepared from each sample, and IC_{50} of the above samples was measured separately, and finally their mean was calculated. BHT, with different concentrations, was considered positive control. All experiments were performed in triplicate (Ghashghaii et al., 2017; Abdoli et al., 2020; Mahdavi et al., 2020).

2.6. Qualitative measurement

The obtained results were loaded into the “SPSS-22” program and evaluated by “one-way ANOVA”, accompanied by a “Duncan post-hoc” check ($p \leq 0.01$).

3. Results and discussion

3.1. Chemical characterization of Fe₃O₄@Thymbra spicata/Au NPs nanocomposite

To rationalize the stepwise synthesis of Fe₃O₄@Thymbra spicata/Au NPs nanocomposite, FT-IR spectra of all the corresponding intermediates have been depicted in Fig. 1. Bare unmodified Fe₃O₄ NPs show a typical absorption at 588 and 638 cm⁻¹ due to Fe-O stretching (Fig. 1a). The characteristic absorption bands of Thymbra spicata extract are represented in Fig. 1b as, 3370 (OH), 2924 (C-H), 1619 (CO), 1400 to 2600 (C=C), 1286 (C-O), 1071 (C-O-C) and 865 cm⁻¹ (O-H) and represent polyols, carbonyls and the C=C bonds of flavonoids and terpenoids (Baghayeri et al., 2018). Fig. 1c, representing the FT-IR spectrum of Fe₃O₄@Thymbra spicata/Au NPs is an amalgamation of both individual component peaks with the slight shifting of characteristic peaks due to strong complexation of Au atoms with the surface functions like OH, CHOH, CH₂OH, C=O etc, which is a clear sign of successful functionalization of the biomolecules and Au NPs over Fe₃O₄ NPs. Interestingly, the strong peak due to Fe-O stretching has also been moved to 572 cm⁻¹ which means that the Au chelation affects the center core (Baghayeri et al., 2018).

The detailed morphological structure, shape and size of the Fe₃O₄@Thymbra spicata/Au NPs nanocomposite were ascertained by SEM and TEM studies. The globular shape nanoparticles can be observed from the SEM images having a mean diameter of a nanometer (Fig. 2). The surface modification over Fe₃O₄ NPs by extract biomolecules can be adjudged from its appearances. There occurs a homogeneous growth of extract over it. The agglomeration of nanocomposite particles can be understood due to manual sample preparation. The bright spots in the image correspond to the Au nanoparticles are easily detectable.

To have the information about the elemental composition of the nanocomposite EDX analysis was carried out. The corresponding profile exhibits Fe, O, C, N and Au atoms (Fig. 3). It demonstrates the successful fabrication of the desired

nanocomposite. Carbon and nitrogen atoms originated from the extract that coated on the surface of magnetic nanoparticles.

The inherent structural features are demonstrated via TEM study of the nanocomposite. The thin layer of the extract surrounding the black-colored Fe₃O₄ NPs can be visible (Fig. 4). The size of the composite particles was by the SEM study and is around 10–15 nm. The tiny black dots correspond to the Au NPs, being ~30 nm in size. In addition, the presence of the extract layer is found effective on *in situ* reductions and immobilization of Au onto the surface of the Fe₃O₄/extract composite. The biomolecular conjugate favors the binding of Au NPs by electrostatic force of attraction and thereby gets stabilized. These data demonstrate the proposed architecture of the material. Moreover, Fig. 4 determines the particle size distribution histograms for Au NPs and Fe₃O₄ NPs whose average size are approximately 32.54 and 9.21 nm respectively.

The crystalline phase of Fe₃O₄@Thymbra spicata/Au NPs nanocomposite was ascertained by XRD and the comparative study is presented in Fig. 5. It demonstrates the typical cubic spinel phase of Fe₃O₄ NPs, the characteristic diffraction peaks are attributed to the (220), (311), (400), (422), (511) and (440) crystal planes (JCPDS No. 19-0629). This also documents that the functionalization over Fe₃O₄ could not change its crystal structure. The additional peaks due to crystalline Au NPs. The peaks appeared at 2 θ = 38.6°, 44.4°, 64.4° and 77.3° corresponds to the face-centered cubic (111), (200), (220) and (311) planes Au crystalline phases (Hamelian et al., 2018). However, the peak intensities are relatively low due to extracting coating over the Fe₃O₄ NPs core.

Magnetic properties of unmodified Fe₃O₄ NPs and Fe₃O₄@Thymbra spicata/Au NPs nanocomposites were determined by VSM analysis at room temperature (Fig. 6). The patterns indicate that they are superparamagnetic nanostructures. The materials exhibit the saturation magnetization (M_s) values of 61.5 and 23.9 emu/g respectively. The gradual decrease in magnetization values is obviously due to the incorporation of extract composites and diamagnetic Au respectively. Still, the final material behaves like a superparamagnet and can be easily attracted by external magnets.

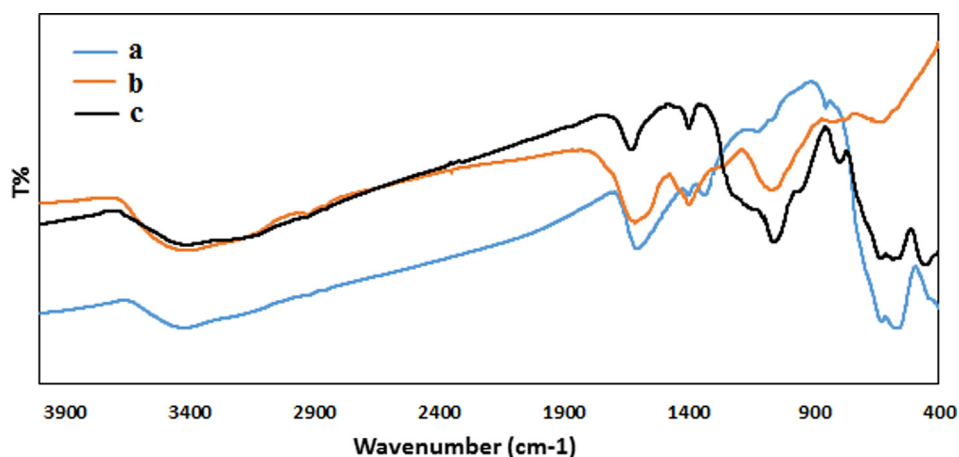


Fig. 1 FT-IR spectra of a) Fe₃O₄, b) Thymbra spicata extract and c) Fe₃O₄@Thymbra spicata/Au NPs.

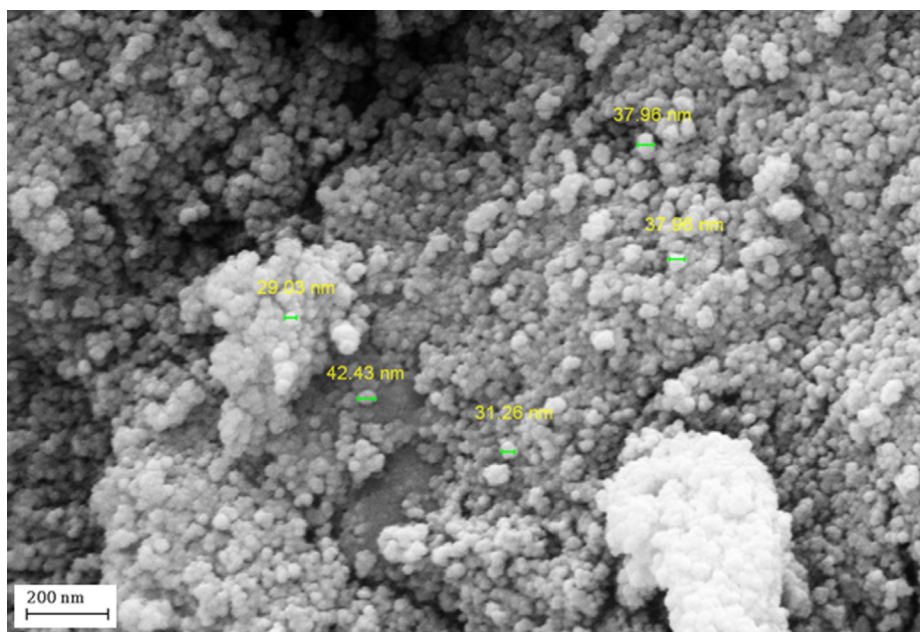


Fig. 2 FESEM image of $\text{Fe}_3\text{O}_4@Thymbra\ spicata/Au$ NPs.

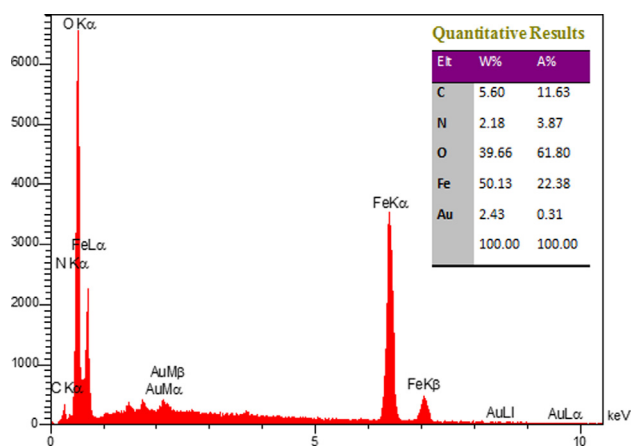


Fig. 3 EDX pattern of $\text{Fe}_3\text{O}_4@Thymbra\ spicata/Au$ NPs.

3.2. Cytotoxicity and anti-ovarian cancer potentials of $\text{Fe}_3\text{O}_4@Thymbra\ spicata/Au$ nanocomposite

In the recent research, the treated cells with several concentrations of the present $\text{Fe}_3\text{O}_4@Thymbra\ spicata/Au$ nanocomposite were examined by MTT test for 48 h regarding the cytotoxicity properties on normal (HUVEC) and common ovarian cancer cell lines i.e., SK-OV-3, SW-626, and PA-1.

The absorbance rate was determined at 570 nm, which indicated extraordinary viability on normal cell line (HUVEC) even up to 1000 $\mu\text{g}/\text{mL}$ for $\text{Fe}_3\text{O}_4@Thymbra\ spicata/Au$ nanocomposite (Fig. 7).

In the case of ovarian cancer cell lines, the viability of them reduced dose-dependently in the presence of $\text{Fe}_3\text{O}_4@Thymbra\ spicata/Au$ nanocomposite. The IC₅₀ of $\text{Fe}_3\text{O}_4@Thymbra\ spicata/Au$ nanocomposite were 185, 251, and 407 $\mu\text{g}/\text{mL}$ against PA-1, SW-626, and SK-OV-3 cell lines, respectively (Table 1).

Among the different parameters of metallic nanoparticles such as, size, texture and nature of surface functions, the size effect is most essential in the anticancer assay using standard cancer cell lines. Previous reports revealed that the anticancer activity increases with a decrease in particle size based on their better penetration ability over the cell lines. It has been surveyed that particle size lower than 50 nm displays better activity in the corresponding cancer cell lines (Abdoli et al., 2020; Mahdavi et al., 2020).

As shown in Figs. 3 and 4 of our study, the average size of $\text{Fe}_3\text{O}_4@Thymbra\ spicata/Au$ nanocomposite is lower than 50 nm.

In the anticancer effects of Au nanoparticles, they have been used to treat several cancers including human lung cancer, mammary carcinoma, uterus cancer, lung epithelial cancer, Lewis lung carcinoma, colon cancer, and human glioma (Abdoli et al., 2020; Mahdavi et al., 2020).

3.3. Antioxidant capacities of $\text{Fe}_3\text{O}_4@Thymbra\ spicata/Au$ NPs nanocomposite

Now, turning our attention to investigate the bioactivity of $\text{Fe}_3\text{O}_4@Thymbra\ spicata/Au$ NPs nanocomposite a concentration-dependent DPPH radical scavenging effect of nanomaterial was observed against BHT as a reference. DPPH process is widely applied to determine the free radical scavenging effect of different antioxidant materials. The DPPH scavenging abilities are known to be because of the hydrogen donating activities of antioxidant materials. When DPPH results are examined, it is observed that it has increased in a dose-dependent manner (Ghashghaii et al., 2017; Abdoli et al., 2020; Mahdavi et al., 2020).

The interaction between $\text{Fe}_3\text{O}_4@Thymbra\ spicata/Au$ NPs nanocomposite and DPPH might have occurred by transferring electrons and hydrogen ions (Abdoli et al., 2020; Mahdavi et al., 2020). The scavenging capacity of the $\text{Fe}_3\text{O}_4@$

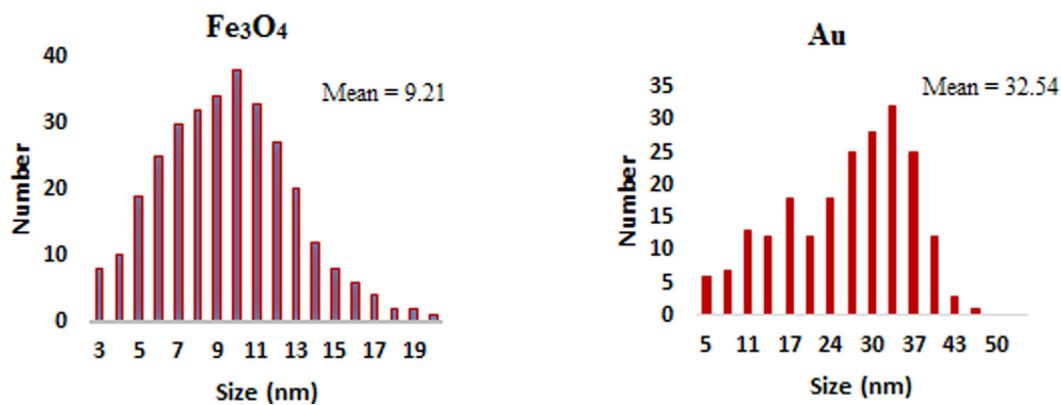
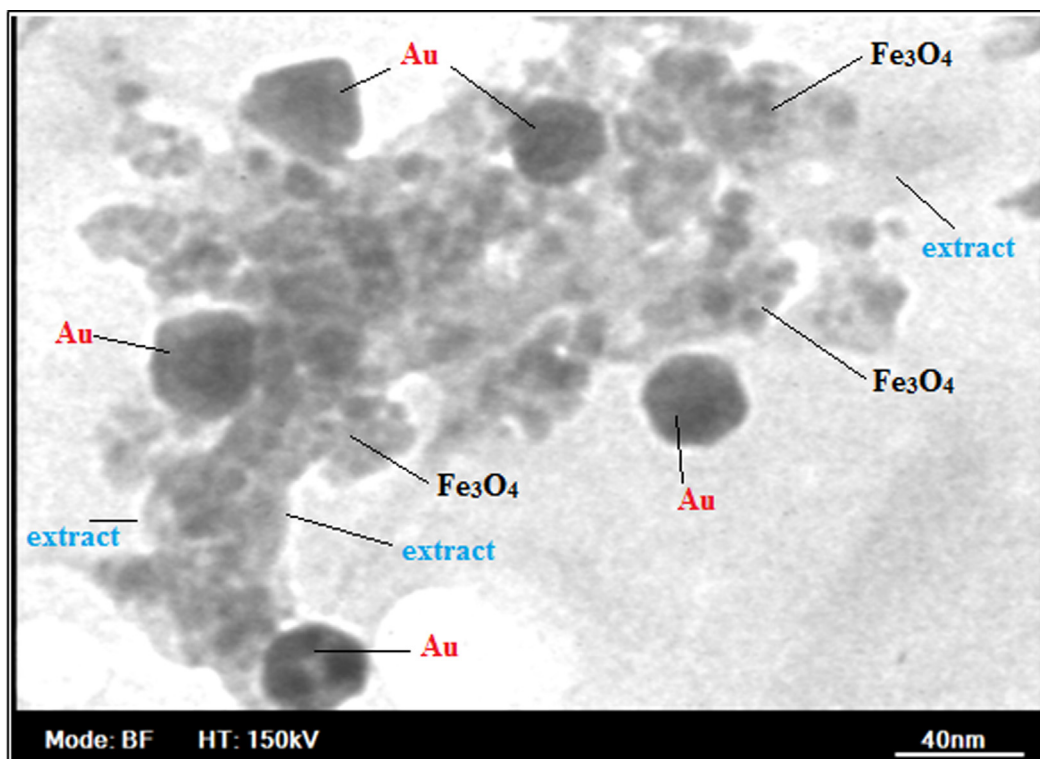


Fig. 4 TEM image of Fe₃O₄@*Thymbra spicata*/Au NPs and particle size distribution histograms for Au NPs and Fe₃O₄ NPs.

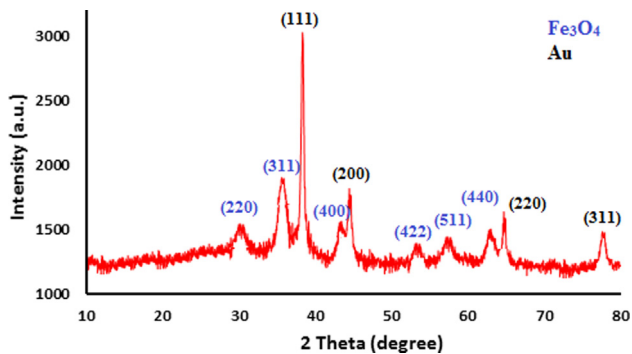


Fig. 5 XRD pattern of Fe₃O₄@*Thymbra spicata*/Au NPs.

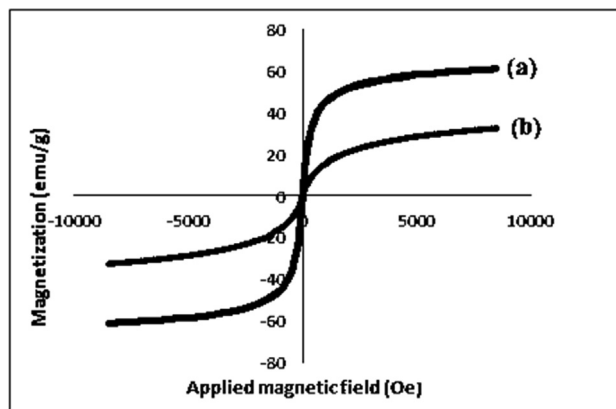


Fig. 6 VSM analysis for a) Fe₃O₄ NPs and b) Fe₃O₄@*Thymbra spicata*/Au NPs.

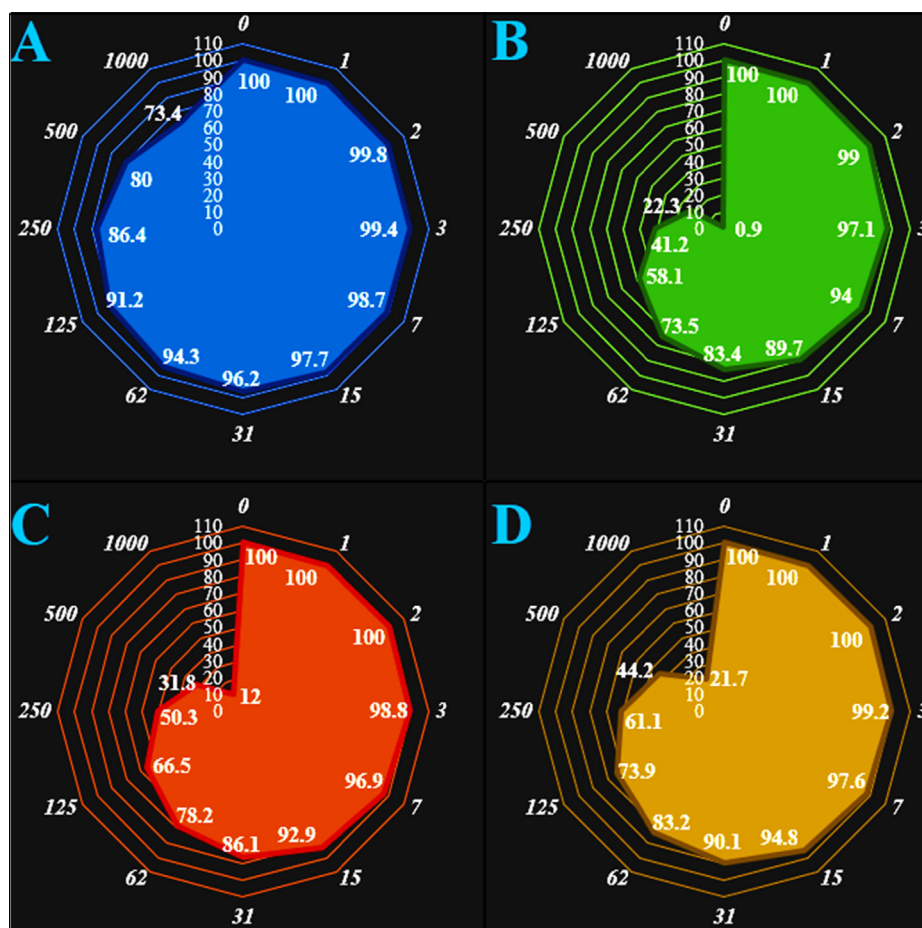


Fig. 7 The anti-human ovarian cancer properties (Cell viability (%)) of $\text{Fe}_3\text{O}_4@Thymbra\ spicata/AuNPs$ (Concentrations of 0–1000 $\mu\text{g}/\text{mL}$) against normal (HUVEC: A) and human ovarian cancer (PA-1 (B), SW-626 (C), and SK-OV-3 (D)) cell lines. The numbers indicate the percent of cell viability at the concentrations of 0–1000 $\mu\text{g}/\text{mL}$ of $\text{Fe}_3\text{O}_4@Thymbra\ spicata/AuNPs$ against several human ovarian cancer cell lines.

Table 1 The IC_{50} of $\text{Fe}_3\text{O}_4@Thymbra\ spicata/AuNPs$ in the anti-human ovarian cancer test.

	HUVEC	PA-1	SW-626	SK-OV-3
IC_{50} ($\mu\text{g}/\text{mL}$)	–	185	251	407

Thymbra spicata/AuNPs nanocomposite and BHT at different concentrations, expressed in terms of percentage inhibition, has been shown in Fig. 8.

In the antioxidant test, the IC_{50} of butylated hydroxytoluene and $\text{Fe}_3\text{O}_4@Thymbra\ spicata/AuNPs$ nanocomposite were 199 and 107 $\mu\text{g}/\text{mL}$, respectively (Table 2).

Au nanoparticles green-mediated show higher antioxidant effects against free radicals formation into the living system (Ghashghaii et al., 2017; Abdoli et al., 2020; Mahdavi et al., 2020). The Au nanoparticles green-formulated have excellent redox properties and have a significant role in free radicals deactivating (Mahdavi et al., 2020). Previous researches have indicated that flavonoids and phenolic compounds attached to the metallic nanoparticles have significant antioxidant properties (Abdoli et al., 2020; Mahdavi et al., 2020).

Likely significant anti-human ovarian cancer potentials of $\text{Fe}_3\text{O}_4@Thymbra\ spicata/AuNPs$ nanocomposite against common ovarian cancer cell lines i.e., SK-OV-3, SW-626, and PA-1 are linked to their antioxidant effects. Similar reports have indicated the antioxidant materials such as metallic nanoparticles especially Au nanoparticles reduce the volume of tumors by removing free radicals (Katata-Seru et al., 2018).

In detail, the high presence of free radicals in the normal cells make many mutations in their DNA and RNA, destroy their gene expression and then accelerate the proliferation and growth of abnormal cells or cancerous cells (Katata-Seru et al., 2018; Sangami and Manu, 2017).

The free radicals high presences in all cancers such as breast, gallbladder, stomach, rectal, liver, gastrointestinal stromal, esophageal, bile duct, small intestine, pancreatic, colon, parathyroid, thyroid, bladder, prostate, testicular, fallopian tube, vaginal, ovarian, hypopharyngeal, throat, lung, and skin cancers indicate the significant role of these molecules in making angiogenesis and tumorigenesis (Sangami and Manu, 2017; Beheshtkhoo et al., 2018).

Many researchers reported that Au nanoparticles green-synthesized have a remarkable role in removing free radicals

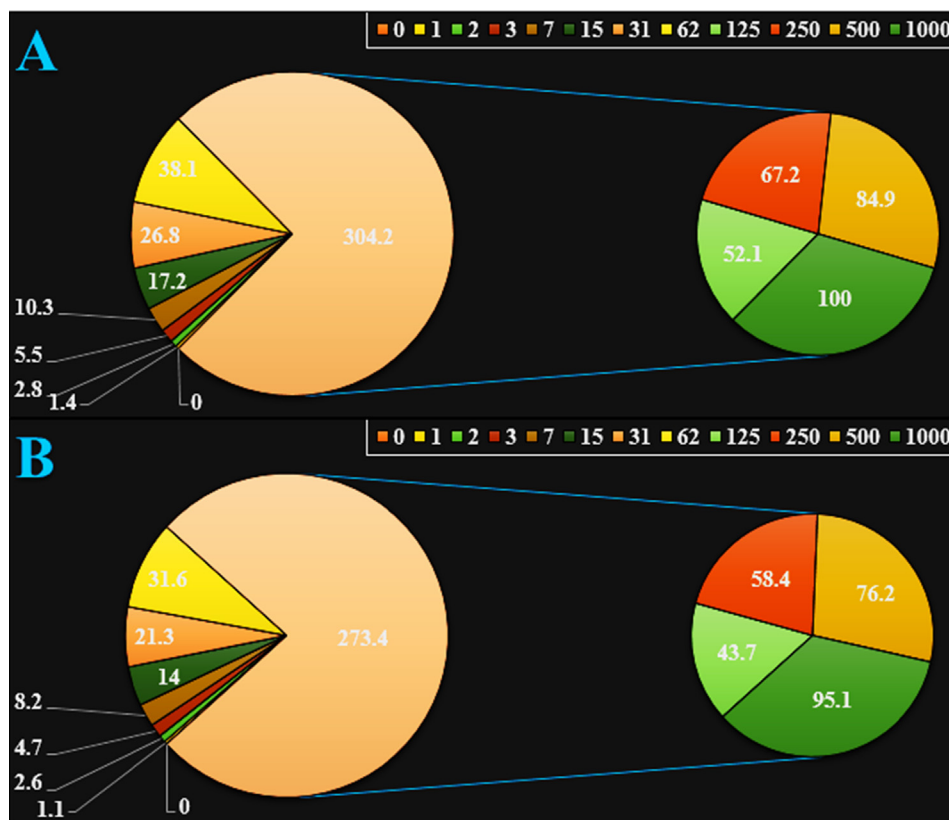


Fig. 8 The antioxidant properties of Fe₃O₄@*Thymbra spicata*/AuNPs (A) and BHT (B) against DPPH. The numbers indicate the percent of free radical (DPPH) inhibition at the concentrations of 0–1000 µg/mL of Fe₃O₄@*Thymbra spicata*/AuNPs (A) and BHT (B).

Table 2 The IC₅₀ of Fe₃O₄@*Thymbra spicata*/AuNPs and BHT in the antioxidant test.

	Fe ₃ O ₄ @ <i>Thymbra spicata</i> /AuNPs	BHT
IC ₅₀ (µg/mL)	107	199

and growth inhibition of all cancerous cells (Radini et al., 2018; Oganessian et al., 1991).

4. Conclusion

In summary we report the green synthesis and anti-ovarian cancer effects of Fe₃O₄@*Thymbra spicata*/Au NPs nanocomposite for the first time. The material was physicochemically characterized using UV–Vis and FT-IR spectroscopy, FESEM, TEM and EDX analysis. The average diameters of the particles were ~30–35 nm. The Fe₃O₄@*Thymbra spicata*/AuNPs nanocomposite revealed excellent antioxidant properties against common free radicals, i.e. DPPH. Also, these nanoparticles had effective anti-ovarian cancer activities dose-dependently against SK-OV-3, SW-626, and PA-1 cell lines without any cytotoxicity on the normal cell line (HUVEC). It seems the Fe₃O₄@*Thymbra spicata*/AuNPs nanocomposite can be used as novel chemotherapeutic supplements or drugs in humans soon.

Declaration of Competing Interest

The authors declare that they have no known competing financial interests or personal relationships that could have appeared to influence the work reported in this paper.

Acknowledgments

The authors extend their appreciation to the deanship of Scientific Research at King Khalid University, Abha, Saudi Arabia, for supporting this work under grant number (R.G. P.2/122/42), and the work was supported by the Taif University Researchers Supporting Project Number (TURSP-2020/99), Taif University, Taif, Saudi Arabia.

References

GBD, Disease and Injury Incidence and Prevalence Collaborators. Global, regional, and national incidence, prevalence, and years lived with disability for 310 diseases and injuries, (2015) 1990–2015: a systematic analysis for the Global Burden of Disease Study 2015. *Lancet*. 388 (2016) 1545–1602.

GBD Mortality and Causes of Death Collaborators. Global, regional, and national life expectancy, all-cause mortality, and cause-specific mortality for 249 causes of death, (2015) 1980–2015: a systematic analysis for the Global Burden of Disease Study 2015. *Lancet*. 388 (2016) 1459–1544.

Ebell, M.H., Culp, M.B.B., Radke, T.J., 2016. *Am. J. Prev. Med.* 50, 384–394.

Grossman, D.C. et al, 2018. *JAMA*. 319, 588–594.

- Gibson, S.J., Fleming, G.F., Temkin, S.M., Chase, D.M., 2016. *Front. Oncol.* 6, 63.
- (a) A. Ghashghaii, M. Hashemnia, Z. Nikousefat, M.M. Zangeneh, A. Zangeneh, *Pharma. Sci.* 23 (2017) 256–263. (b) S. Goorani, N. Shariatifar, N. Seydi, A. Zangeneh, R. Moradi, B. Tari, F. Nazari, M.M. Zangeneh, *Oriental Pharm. Exp. Med.* 19 (2019) 403–413. (c) A.R. Jalalvand, M. Zhaleh, S. Goorani, M.M. Zangeneh, N. Seydi, A. Zangeneh, R. Moradi, *J. Photochem. Photobiol. B: Biol.* 192 (2019) 103–112. (d) R. Moradi, M. Hajjalilani, S. Salmani, M. Almasi, A. Zangeneh, M.M. Zangeneh, *Compar. Clin. Pathol.* 28 (2019) 1205–1211. (e) K. Rashidi, M. Mahmoudi, G. Mohammadi, M.M. Zangeneh, S. Korani, H.C. Goicoechea, H.-W. Gu, A.R. Jalalvand, *Int. J. Biol. Macromol.* 120 (2018) 587–595. (f) H. Sherkatolabbasieh, L. Hagh-Nazari, S. Hagh-Nazari, N. Goodarzi, M.M. Zangeneh, A. Zangeneh, *Arch. Biol. Sci.* 69 (2017) 535–543.
7. (a) M. Abdoli, K. Sadrjavadi, E. Arkan, M.M. Zangeneh, S. Moradi, A. Zangeneh, M. Shahlaei, S. Khaledian, *J. Drug Deliv. Sci. Technol.* 60 (2020) 102044. (b) A. Ahmeda, A. Zangeneh, M. M. Zangeneh, *Appl. Organomet. Chem.* 34 (2020) e5290. (c) L. Dou, X. Zhang, M.M. Zangeneh, Y. Zhang, *Bioorg. Chem.* 106 (2020) 104468. (d) Y. Han, Y. Gao, X. Cao, M.M. Zangeneh, S. Liu, J. Li, *Int. J. Biol. Macromol.* 164 (2020) 2974–2986. (e) M. Ishaq, P. Taslimi, Z. Shafiq, S. Khan, R.E. Salmas, M.M. Zangeneh, A. Saeed, A. Zangeneh, N. Sadeghian, A. Asari, H. Mohamad, *Bioorg. Chem.* 100 (2020) 103924. (f) Y. Li, N. Li, W. Jiang, G. Ma, M.M. Zangeneh, *Int. J. Biol. Macromol.* 163 (2020) 2162–2171.
- (a) B. Mahdavi, S. Paydarfard, M.M. Zangeneh, S. Goorani, N. Seydi, A. Zangeneh, *Appl. Organomet. Chem.* 34 (2020) e5248. (b) B. Mahdavi, S. Saneii, M. Qorbani, M. Zhaleh, A. Zangeneh, M.M. Zangeneh, E. Pirabbasi, N. Abbasi, H. Ghaneialvar, *Appl. Organomet. Chem.* 33 (2019) e5164. (c) N. Seydi, B. Mahdavi, S. Paydarfard, A. Zangeneh, M.M. Zangeneh, F. Najafi, A.R. Jalalvand, E. Pirabbasi, *Appl. Organomet. Chem.* 33 (2019) e5009. (d) A. Sujayev, P. Taslimi, E. Garibov, M. Karaman, M. M. Zangeneh, *Bioorg. Chem.* 104 (2020) 104216. (e) T. Sun, J. Gao, H. Shi, D. Han, M.M. Zangeneh, N. Liu, H. Liu, Y. Guo, X. Liu, *Int. J. Biol. Macromol.* 165 (2020) 787–795. (f) R. Tahvilian, M.M. Zangeneh, H. Falahi, K. Sadrjavadi, A.R. Jalalvand, A. Zangeneh, *App. Organomet. Chem.* 33 (2019) e5234.
- Gawande, M.B., Branco, P.S., Varma, R.S., 2013. *Chem. Soc. Rev.* 42, 3371–3393.
- Lotfi, S., Veisi, H., 2019. *Mater. Sci. Eng. C* 105, 110112–110122.
- Sanli, S., Ghorbani-Zamani, F., Moulahoum, H., Gumus, Z.P., Coskunol, H., Demirkol, D.O., Timur, S., 2020. *Anal. Chem.* 92, 1033–1040.
- Rossi, L.M., Costa, N.J., Silva, S.F.P., Wojcieszak, R., 2014. *Green Chem.* 16, 2906–2933.
- Veisi, H., Mirzaei, A., Mohammadi, P., 2019. *RSC Adv.* 9, 41581–41590.
- (a) S. Hemmati, M. Hekmati, D. Salamat, M. Yousefi, B. Karmakar, H. Veisi, *Polyhedron* 179 (2020) 114359–114364. (b) H. Veisi, *Curr. Org. Chem.* 15 (2011) 2438–2468.
- Baghayeri, M., Amiri, A., Alizadeh, Z., Veisi, H., Hasheminejad, E., 2018. *J. Electroanal. Chem.* 810, 69–77.
- Veisi, H., Sedrpoushan, A., Faraji, A.R., Heydari, M., Hemmati, S., Fatahi, B., 2015. *RSC Adv.* 5, 68523–68530.
- (a) Katifelis H, Mukha I, Bouziotis P, Vityuk N, Tsoukalas C, Lazaris AC, Lyberopoulou A, Theodoropoulos GE, Efstathopoulos EP, Gazouli M, *Int J Nanomedicine.* 15 (2020) 6019–6032; (b) H. Veisi, T. Ozturk, B. Karmakar, T. Tamoradi, S. Hemmati, *Carbo. Polym.* 235 (2020) 115966.
- (a) Katifelis, H. Lyberopoulou, A. Mukha, I. Vityuk, N. Grodzyuk, G. Theodoropoulos, G.E. Gazouli, E.P. Efstathopoulos, M. Artif Cells Nanomed Biotechnol. 46 (2018) S389–S398; (b) Veisi, H. Hemmati, S. Safarimehr, P. J. Catal. 365 (2018) 204–212.
- (a) Cheng, L. Zhang, D. Liao, Y. Lib, F. Zhang, H. Xiang, Q. J. Colloid Interf. Sci. 555 (2019) 94; (b) Yang, Y. Li, F. Chen, J. Fan, J. Xiang, Q. ChemSusChem, 13 (2020) 1979; (c) Li, Y. Li, X. Zhang, H. Fan, J. Xiang, Q. J. Mater. Sci. Technol. 56 (2020) 69; (d) Gawande, M. B. Branco, P. S. Varma. R. S. Chem. Soc. Rev. 42 (2013) 3371–3393
- Mirfakhraei, S., Hekmati, M., Hosseini-Eshbala, F., Veisi, H., 2018. *New J. Chem.* 42, 1757–1761.
- Li Y, Lin T, Luo Y, Qiangqiang Liu, Wenwu Xiao, Wenchang Guo, Diana Lac, Hongyong Zhang, Caihong Feng, Sebastian Wachsmann-Hogiu, Jeffrey H. Walton, Simon R. Cherry, Douglas J. Rowland, David Kukis, Chongxian Pan & Kit S. Lam. *Nat Commun.* 5 (2014) 4712.
- Mu, X., Zhang, F., Kong, C., 2017. *Hongmei Zhang, Wenjing Zhang, Rui Ge, Yi Liu. Jinlan Jiang. Int. J. Nanomedicine.* 12, 2899–2911.
- Lian, H.Y., Hu, M., Liu, C.H., Yamauchi, Y., Wu, K.C.W., 2012. *Chem. Commun.* 48, 5151–5153.
- Mcnamara, K., Tofail, S.A., 2015. *Phys. Chem. Chem. Phys.* 17, 27981–27995.
- Tassa, C., Shaw, S.Y., Weissleder, R., 2011. *Acc. Chem. Res.* 44, 842–852.
- Lutz, J.F., Stiller, S., Hoth, A., Kaufner, L., Pison, U., Cartier, R., 2006. *Biomacromolecules.* 7, 3132–3138.
- Kohler, N., Fryxell, G.E., Zhang, M., 2004. *J. Am. Chem. Soc.* 126, 7206–7211.
- Masoudi, A., Madaah Hosseini, H.R., Shokrgozar, M.A., Ahmadi, R., Oghabian, M.A., 2012. *Int. J. Pharm.* 433, 129–141.
- Ban, Z., Barnakov, Y.A., Li, F., Goluba, V.O., O’Conno, C.J., 2005. *J. Mater. Chem.* 15, 4660–4662.
- Chen, M., Yamamuro, S., Farrell, D., Majetich, S.A., 2003. *J. Appl. Phys.* 93, 7551–7553.
- Zhou, T., Wu, B., Xing, D., 2011. *J. Mater. Chem.* 22, 470–477.
- Awual, M.R., Khraisheh, M., Alharthi, N.H., Luqman, M., Islam, A., Rezaul Karim, M., Rahman, M.M., Khaleque, M.A., 2018. *Chem. Eng. J.* 343, 118–127.
- Veisi, H., 2019. *Polyhedron* 159, 212–216.
- Hamelian, M., Varmira, K., Veisi, H., 2018. *J. Photochem. Photobiol. B: Biol.* 184, 71–79.
- Katata-Seru, L., Moremedi, T., Aremu, O.S., 2018. *Indra Bahadur. J. Mol. Liq.* 256, 296–304.
- Sangami, S., Manu, M., 2017. *Environ. Technol. Innov.* 8, 150–163.
- Beheshtkhoo, N., Kouhbanani, M.A.J., Savardashtaki, A., Amani, A. M., Taghizadeh, S., 2018. *Appl. Phys. A* 124, 363–369.
- Radini, I.A., Hasan, N., Malik, M.A., Khan, Z., 2018. *J. Photochem. Photobiol. B* 183, 154–163.
- (a) Ángeles-Pascual, A. Piñón-Hernández, J.R. Estevez-González, M. Pal, U. Velumani, S. Pérez, R. Esparz, R. Mat. Charac., 142(2018) 237–244; (b) Madrid, S.I.U. Pal, U. Kang, Y.S. Kim, J. Kwon, H. Kim, *J. Nanoscale Res. Lett.* 10 (2015) 217; (c) Lu, Q. Dai, X. Zhang, P. Tan, X. Zhong, Y. Yao, C. Song, M. Song, G. Zhang, Z. Peng, G. Guo, Z. Ge, Y. Zhang, K. Li, Y. *Int J Nanomedicine* 13 (2018) 2491–2505; (d) Cai, J. Miao, Y.Q. Li, L. Fan, H.M. *Int. J. Mol. Sci.* 19 (2018) 4049; (e) Li, Y. Liu, J. Zhong, Y. Zhang, J. Wang, Z. Wang, L. An, Y. Lin, M. Gao, Z. Zhang, D. *Int. J. Nanomedicine.* 6 (2011) 2805–2819.
- Oganessian G, Galstyan A, Mnatsakanyan V, Paronikyan R. V., Yu. Ter-Zakharyan *Z. Chem. Nat.* 27 (1991) 247–247.